Local O_δ probing in the high-T_c superconductor $HgBa_2CuO_{4+\delta}$

J. G. Correia* and ISOLDE Collaboration
CERN-EP/SC, CH-1211 Geneva 23, Switzerland

J. P. Araújo
IFIMUP, Departamento de Física, FCP, Rua do Campo Alegre 687, P-4150 Porto, Portugal

S. M. Loureiro
Department of Chemistry, Princeton University, Princeton, New Jersey 08544

P. Toulemonde, S. Le Floch, P. Bordet, and J. J. Capponi
Laboratoire de Cristallographie, CNRS, Avenue des Martyrs 25, F-38042 Grenoble Cedex 9, France

R. Gatt
Department of Physics (M/C 273), 2168 SES, University of Illinois, Chicago, Illinois 60612

W. Tröger, B. Ctortecka, and T. Butz
Fakultät für Physik und Geowissenschaften, Universität Leipzig, Linnéstraße 5, D-04103 Leipzig, Germany

H. Haas
Bereich Festkörperphysik, Hahn-Meitner-Institut Berlin GmbH, D-14109 Berlin, Germany

J. G. Marques and J. C. Soares
Instituto Tecnológico e Nuclear, Estrada Nacional 10, P-2685 Sacavém, Portugal
and CFNUL, Avenida Professor Gama Pinto 2, P-1699 Lisboa Codex, Portugal
(Received 27 October 1999)

Electric-field gradients on mercury sites of the $HgBa_2CuO_{4+\delta}$ high-T_c superconductor were measured with the perturbed angular correlation technique and interpreted with *ab initio* calculations. Under oxygen annealing, an asymmetric electric-field gradient has been assigned to the presence of single oxygen atoms, O_δ, which are located in the Hg planes. These experiments provide an atomic scale tool for studying charge-density variations occuring in the neighborhood of the Hg atoms, which can be induced, particularly, by pointlike defects.

I. INTRODUCTION

Since the compounds of the family $HgBa_2Ca_{(n-1)}Cu_nO_{(2n+2+\delta)}$ have been synthesized they have been revealed as one of the most interesting systems among high-T_c superconductors.[1] These compounds crystallize in a tetragonal lattice (space group $P4/mmm$) with lattice parameters $a \approx a_{\text{perovskite}} \approx 3.88$ Å and $c \approx 9.5 + 3.2(n-1)$ Å (Fig. 1). While the bond between Hg and the apical oxygen O(2) seems to be quite strong and incompressible, the Cu-O(2) bond length is pressure dependent. At 30 GPa a critical temperature (T_c) as high as 164 K can be achieved in the Hg-1223 ($n=2$) compound.[2] Such facts created the expectation that precise measurements of the structural properties would provide a better understanding of the charge-transfer mechanisms that generate carriers in the CuO_2 superconducting planes. However, it was soon realized that the Hg planes are particularly disordered. In fact, there are Hg vacancies, impurities replacing Hg and the nonstoichiometric oxygen, O_δ, that is considered to be the dopant that regulates T_c.[3] Meanwhile, structural distortions of the polaronic type and of charge inhomogeneity in the CuO_2 layers have become the main issue of research in the field of superconductivity. Neutron-diffraction studies performed on powder samples[4] as well as more local methods such as extended x-ray-diffraction fine structure[5] pointed to the existence of local distortions in these compounds. So far it is not clear if

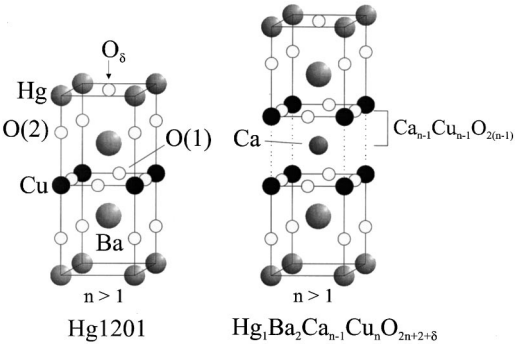

FIG. 1. Schematic view of the Hg1201 (left) and $HgBa_2Ca_{n-1}Cu_nO_{2n+2+\delta}$ (right) crystalline structures.

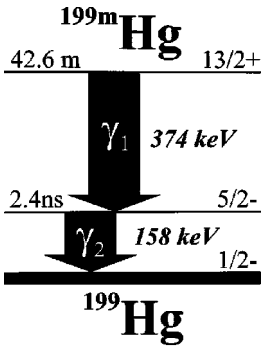

FIG. 2. γ-γ cascade in the decay of the isomeric state of ^{199m}Hg ($T_{1/2}=42.6$ min) to the ^{199}Hg ground state.

such effects are linked to the superconductivity mechanism or are simply due to crystal-impurity chemical effects.

Nuclear hyperfine techniques like nuclear magnetic resonance (NMR) and nuclear quadrupole resonance (NQR) are extremely useful in providing atomic scale information on the probe-element interactions with the lattice host.[6] In particular, the measurement of the electric-field gradient (EFG) at specific probe-element nuclei provides direct information about the local charge distribution. The EFG is highly sensitive to the probe's local environment and can thus provide a fingerprint of the lattice site or of a defect that is located in the probe's neighborhood. Unfortunately, NQR on ^{201}Hg, the only stable isotope with spin$>1/2$, is not too promising and very few experiments on different materials with ^{201}Hg were reported since 1954 by Dehmelt.[7] Alternatively, time differential perturbed angular correlation (PAC) of γ rays, from the decay of the 42.6 min half-life ^{199m}Hg isomeric state (Fig. 2), is a very well-suited method for this purpose. PAC measures the EFG that is generated by the deviation from cubic symmetry of the charge distribution around the probe nuclei.[8] In the case of ^{199m}Hg, the interaction of the EFG with the quadrupole moment $Q=0.674\pm0.077$ b of the $5/2^-$ 158 keV intermediate state of the cascade leads to this level energy splitting.[9] That induces a time-dependent modulation $G(t)$ on the intensity of the angular correlation between the first gamma ray (γ_1), which populates the 158 keV intermediate state, and the second gamma-ray (γ_2) emitted when the intermediate state decays to the ^{199}Hg ground state. Experimentally, $G(t)$ will be observed as a modulation that is superimposed on the half-life decay curve of the 158 keV state.

In the present work, the PAC technique was applied for the first time to investigate the EFG's on Hg sites of the Hg1201 ($n=1$) compound as a function of the oxygen doping concentration.

II. EXPERIMENTAL

Hg1201 powder samples were produced by solid-state reaction under high pressure (18 kbar) and high temperature (1193 K) of a mixture of a precursor with the nominal composition Ba_2CuO_y and the stoichiometric amount of HgO (in Loureiro[10,11(a)]). The mixture was placed inside a gold capsule for the high pressure–high temperature synthesis. In order to reduce the O_δ concentration the synthesized material was annealed at 523 K under 1 bar Ar flow during 24 h. Thereafter, to obtain homogeneous samples the annealed powder was thoroughly mixed in an agate mortar and packed in self-sustained pellet disks, each one with approximately 5 mm diameter and 0.5 mm thickness. To avoid contamination or degradation the pellets were stored and manipulated in dry Ar atmosphere. Small samples with approximately 0.5 mm^3 were cut out of the disk to be used in the PAC experiments.

The ^{199m}Hg isotope was produced at the ISOLDE/CERN (Ref. 12) on-line mass separator and implanted into the samples with 60 keV energy under vacuum at room temperature (RT). The ^{199m}Hg projected range is $R_P=17$ nm with the straggling of $\sigma=7$ nm.[13] In order to produce a homogenous implanted zone and to minimize the implantation damage the ^{199m}Hg beam was swept to achieve a relatively low dose of 5×10^{11} at/cm^2. Under these conditions, 15 min annealing at 473 K suffices to eliminate the implantation damage in the ^{199}Hg neighborhood. The experimental setup was equipped with a high-precision temperature controlled furnace where the annealing can be performed during the measurement under gas flow.[14] For controlling the sample quality and the oxygen concentration, x-ray-diffraction measurements of the lattice parameters were done before and after the PAC experiments on each sample (Table I).

The PAC experiments were performed with a highly efficient 6-detector TDPAC-camera equipped with conical shaped BaF_2-scintillators, which has 650 ps (full width at half maximum) time resolution for the ^{199m}Hg cascade.[15] In this setup 6 γ_1-γ_2 coincidence time spectra from detector pairs at $\theta=180°$ and 24 coincidence time spectra from detector pairs at $\theta=90°$ are simultaneously recorded. With the coincidence countrates, $N_j(180°,t)$, $j=1-6$, and $N_i(90°,t)$, $i=1-24$, for each detector pair, the experimental ratio $R(t)$ is formed [Eq. (1)]:

TABLE I. a and c lattice parameters measured by x-ray diffraction on the samples before and after the ^{199m}Hg implantation and the PAC experiments. δ was estimated from the lattice parameter a as presented in Fig. 5 and explained in the text.

Experiment: T_A, t_A, gas[a]	a (Å)	c (Å)	T_C (K)	δ (%)
As-prepared	3.8785 ± 0.0004	9.4998 ± 0.0013	88	10.0
First exp.: 490 K, 220 min, Ar	3.8801 ± 0.0005	9.502 ± 0.002	Not measured	7.9
Third exp.: 490 K, 180 min, Ar	3.8820 ± 0.0007	9.506 ± 0.002		9.1
Second exp.: 490 K, 200 min, O_2	3.8768 ± 0.0002	9.4981 ± 0.0007		10.7
Fourth exp.: 490 K, 240 min, O_2	3.8758 ± 0.0009	9.495 ± 0.003		11.1

[a]T_A=annealing temperature, t_A=annealing time.

$$R(t)=2\frac{\sqrt[6]{\Pi_j^6 N_j(180°,t)}-\sqrt[24]{\Pi_i^{24} N_i(90°,t)}}{\sqrt[6]{\Pi_j^6 N_j(180°,t)}+2\sqrt[24]{\Pi_i^{24} N_i(90°,t)}}. \quad (1)$$

This ratio eliminates the half-life exponential component, revealing the perturbation function that contains all the relevant information. For each angle θ, the angular correlation functions $W(\theta,t)$ are calculated numerically by taking into account the full Hamiltonian for the nuclear quadrupole hyperfine interaction.[8,16] Equation (2) defines the theoretical function $R_{\rm fit}(t)$, whose parameters are fitted to the experimental $R(t)$ function:

$$R_{\rm fit}(t)=2\,\frac{W(180°,t)-W(90°,t)}{W(180°,t)+2W(90°,t)}. \quad (2)$$

For a γ-γ cascade with the intermediate level of spin $I=5/2$, three frequencies are observable per EFG. From these frequencies the coupling constant of the interaction $\nu_Q=eQV_{zz}/h$ and the asymmetry parameter $\eta=(V_{xx}-V_{yy})/V_{zz}$ are extracted. V_{zz} is the principal component of the EFG tensor that is produced by the charge distribution outside the probe nucleus. V_{yy} and V_{xx} are the components of the tensor along the y and x axes, which are chosen according to $|V_{zz}|>|V_{yy}|>|V_{xx}|$. In the case of an interaction with randomly distributed defects a distribution of frequencies is observed, which broadens the frequency spectrum and thus attenuates the $R(t)$ function. In this work only weak distributions are found, which were assumed to be Lorentzian-like. These are characterized by the average value ν_Q and standard deviation σ_Q, which depend on the density and variety of the lattice defects.[17]

III. RESULTS

A. Experiments

Figure 3 shows the experimental $R(t)$ functions (left) and the corresponding Fourier transforms (FT's) (right) of four experiments that were performed on the described samples. In order to enhance the quality of the fits, which are represented by continuous lines in the $R(t)$ spectra, the corresponding Fourier transforms of the theoretical functions are included as thicker lines on the FT plots. In order to improve statistics, the summed data taken under the same experimental conditions are also included in Fig. 3. Table II shows the fit parameters. Italic characters are subsequently adopted when referring to fit parameters of added spectra.

When annealing at 489 K under dry Ar flow, the spectra of the experiments 1 and 3 show a frequency triplet that reveals one axially symmetric EFG_1, characterized by $\nu_{Q1}=1448\pm5$ MHz and $n_1=0$. This clearly corresponds to ^{199m}Hg nuclei placed on regular sites of the Hg1201 lattice with local tetragonal symmetry. A small attenuation of the $R(t)$ spectra is still observable that is characterized by $\sigma_{Q1}=35\pm3$ MHz. Most likely the long-range disorder of the Hg planes produces this small EFG distribution.

When annealing at 489 K under oxygen flow, the spectra of experiments 2 and 4 exhibit three frequency triplets. Two of them correspond to slightly different EFG's. A fraction $f_1=66\pm5\%$ of Hg nuclei interact with the same axially symmetric EFG_1 as above, while a fraction $f_2=23\pm4\%$ of

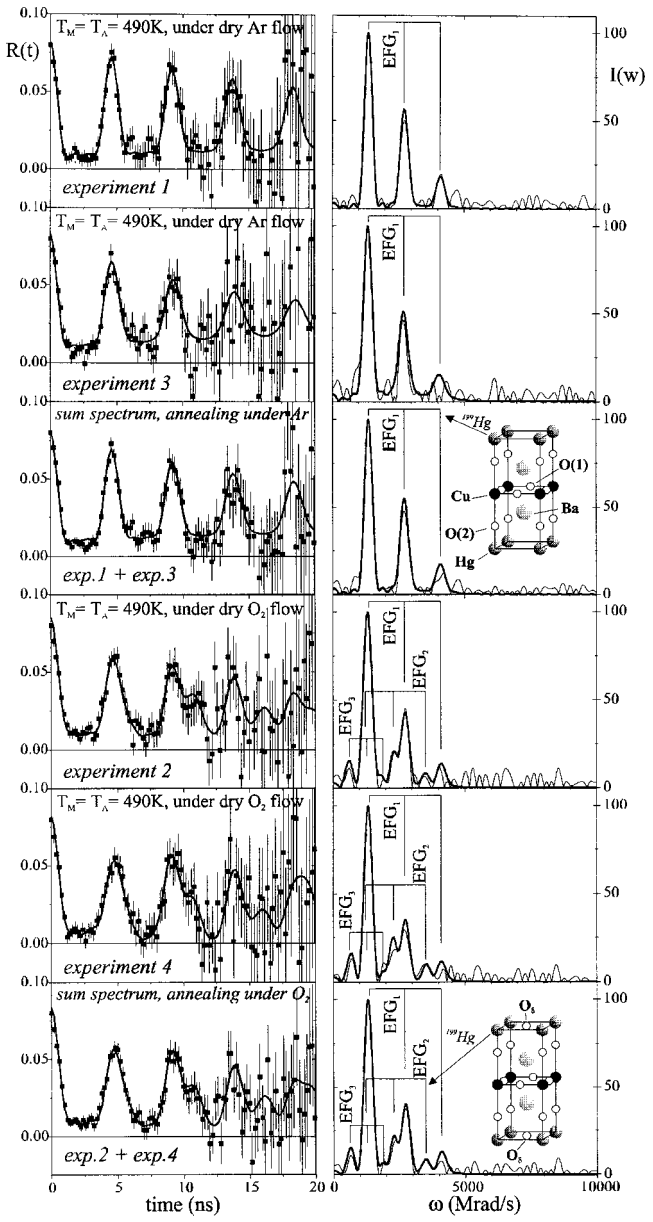

FIG. 3. PAC time spectra $R(t)$ (left) and the corresponding Fourier transforms of the $R(t)$ functions (right). In the $R(t)$ and the Fourier spectra the thicker lines represent the fit function and the Fourier transform of the fit function, respectively.

^{199}Hg nuclei interact with a nonaxially symmetric EFG_2, characterized by $\nu_{Q2}=1229\pm14$ MHz and $\eta_2=0.21\pm0.04$. Thus a large fraction of Hg atoms are on lattice sites with lower than tetragonal symmetry. A third EFG_3 was observed which is characterized by $f_3=11\pm2\%$ and $\nu_{Q3}=673\pm21$ MHz. In this case the η_3 parameter was set equal to zero, since the small fraction and the overlap of other frequencies does not allow us to determine it unambiguously. Due to the small attenuation of the $R(t)$ spectra $\sigma_{Q2}=\sigma_{Q3}=0$ was further assumed for the sake of simplicity.

B. EFG calculations

In order to interpret the experimental data, EFG calculations were performed with the *ab initio full-potential-linearized-augmented-plane-wave* (FLAPW) electronic

TABLE II. EFG fitting parameters of the PAC experiments. Values expressed in italic characters are obtained by fitting the sum of the spectra, which were taken under the same experimental conditions.

Experiment	$T_M = T_A$[a] (K)	t_A[b] (min)	gas	f_1 (%)	ν_{Q1} (MHz)	$\lvert V_{zz}\rvert_1$ (V/Å^2)	η_1	σ_1 (MHz)	f_2 (%)	ν_{Q2} (MHz)	$\lvert V_{zz}\rvert_2$ (V/Å^2)	η_2	σ_2[c] (MHz)	f_3 (%)	ν_{Q3} (MHz)	$\lvert V_{zz}\rvert_3$ (V/Å^2)	η_3[c]	σ_3[c] (MHz)
First exp.	490	~220	Ar	100	1455	893	0	28										
					±4	±102		±3										
Third exp.	490	~180	Ar	100	1437	882	0	58										
					±10	±101		±14										
Sum of first and third exp.	*490*		*Ar*	*100*	*1448*	*888*	*0*	*35*										
					±5	*±102*		*±3*										
Second exp.	490	~200	O_2	68	1456	893	0	29	21	1233	757	0.18	0	11	641	393	0	0
				±6	±8	±102		±2	±5	±19	±87	±0.04		±2	±34	±50		
Fourth exp.	490	~240	O_2	61	1456	893	0	29	27	1224	751	0.27	0	12	704	432	0	0
				±7	±8	±102		±2	±4	±17	±86	±0.01		±4	±16	±50		
Sum of second and fourth exp.	*490*		O_2	*66*	*1456*	*893*	*0*	*29*	*23*	*1229*	*754*	*0.21*	*0*	*11*	*673*	*413*	*0*	*0*
				±5	*±7*	*±102*		*±2*	*±4*	*±14*	*±87*	*±0.04*		*±2*	*±21*	*±49*		

[a] T_M = PAC measurement temperature, T_A = annealing temperature.
[b] t_A = annealing time.
[c] Parameters set to zero during the fits, explained in text.

FIG. 4. Representation of the Hg planes of Hg1201 as viewed along the *c* axis. Shaded regions represent the *undoped* ($\delta=0$), *overdoped* ($\delta=0.25$), and *saturated* $Cf(a)$ and $Cf(b)$ ($\delta=0.5$) supercells, which were used for the EFG calculations. Ellipses which enclose italic characters show the position of rows of Ba*a*, Ba*b*, Ba*c*, and O(1)*a*, O(1)*b*, O(1)*c* atoms, which are located out of the Hg planes, as it is explained in the text.

structure method using the *local-density approximation*.[18] This method allows, in particular, the computation of hyperfine parameters in crystalline solids by only requiring the lattice constants as input parameters, which in this work were taken from neutron diffraction experiments [Table I in Ref. 11(b)]. To account for the O_δ doping, several supercells were considered with composition $Hg_mBa_{2m}Cu_mO_{4m+n}$. They are denoted as *undoped* for $\delta=0$ ($m=1$, $n=0$), *overdoped* for $\delta=0.25$ ($m=4$, $n=1$) and *saturated* for $\delta=0.5$ ($m=2$, $n=1$). Figure 4 shows a schematic view of the supercells projected along the [001] axis onto the Hg planes. Table III presents the EFG parameters obtained for the *undoped* case, for each lattice element. They are in good agreement with previous calculations by Singh.[19] It should be stressed that the present calculations were performed by setting the internal structure parameter of the apical O(2) oxygen to $z_{O(2)}=0.2061$, as obtained from neutron diffraction data. By slightly increasing/decreasing $z_{O(2)}$ a strong variation of the EFG at the Hg site was found, e.g., $\lvert\partial V_{zz}/\partial z_{O(2)}\rvert_{Hg}\approx 2\times10^4$ V/Å^2 (see Table III). As expected, the EFG at the O(2) site has also strongly changed. More surprising is the big influence of small $z_{O(2)}$ variations on the EFG at the Ba site, while for Cu and O(1) the results are virtually unchanged. Additional information can be obtained from the calculated forces acting on O(2). When allowing the apical oxygen to relax, while keeping the lattice parameters unchanged elsewhere, one would obtain a theoretical value for $z_{O(2)}=0.2086$, somewhat different from the experimental data.

In order to calculate the effect of the oxygen doping in the Hg planes, two *saturated* $\delta=0.5$ supercells (a) and (b) were constructed (Fig. 4). These correspond to an unrealistic high

TABLE III. EFG parameters obtained from FLAPW first-principles calculations for the *undoped* ($\delta=0$) cell. For those positions with a calculated value of $\eta=0$, the principal system of axis (psa) of the EFG has the *z* axis parallel to [001] and the *x* and *y* axes parallel to the [100] and [010] directions. For the O(1) position the *z* axis of the psa of the EFG is parallel to [100], along the Cu-O(1) bond, the *x* axis is parallel to [001] and the *y* axis is parallel to [010]. $a=3.88881$ Å, $c=9.5398$ Å, $z_{Ba}=0.302$.

		$z_{O(2)}$					
		Standard 0.2061		Compressed 0.2011		Expanded 0.2161	
Element	V_{ii}	(V/Å^2)	(η)	(V/Å^2)	(η)	(V/Å^2)	(η)
Hg	V_{zz}	−818.8	0	−929.4	0	−653.4	0
Ba	V_{zz}	60.4	0	48.4	0	85.6	0
Cu	V_{zz}	−28.4	0	−28.2	0	−27	0
	V_{xx}	−43.3		−42.7		−45.6	
O(1)	V_{yy}	−83.9	0.318	−84.6	0.329	−83.2	0.292
	V_{zz}	127.2		127.3		128.8	
O(2)	V_{zz}	141	0	128.8	0	163	0

degree of doping and describe two different configurations of two O_δ atoms located around every Hg in relative positions $(-1/2,-1/2,z_{Hg})(1/2,1/2,z_{Hg})[Cf(a)]$ and $(1/2,-1/2,z_{Hg})(1/2,1/2,z_{Hg})[Cf(b)]$. In this way the EFG's at the Hg site produced by two O_δ neighbors are estimated to be nonaxially symmetric and much weaker then the one found for the *undoped* case (Tables III and IV). In $Cf(a)$ and $Cf(b)$ two sites exist for Ba, e.g., Ba*a* and Ba*b*, which are located in and out of O_δ rows parallel to the $\overline{[001]}$ axis. O(1) has only one equivalent site, O(1)*b*, in $Cf(a)$, while it has three inequivalent sites in $Cf(b)$:O(1)*a* located *in between* two O_δ rows, O(1)*b* located near *only one* O_δ row, and O(1)*c* located in sites *without* O_δ rows nearby.

Due to Fermi level changes, the EFG at the Cu site is significantly changed between the *undoped* and the *saturated* $Cf(a)$ and $Cf(b)$ simulations. The EFG is most affected at the Ba*a* site where even the sign of V_{zz} has changed, due to the presence of the nearby O_δ atom (Table IV).

In order to study a more realistic case with smaller oxygen doping concentration, the EFG at the Hg site with only one O_δ neighbor in the tetragonal plane has to be calculated. The primary difference between the *undoped* and the $Cf(a)$ *saturated* supercells is the presence of two O_δ atoms as neighbors to Hg. Since only moderate changes of the EFG at the Hg site are calculated, a first guess for the effect of one O_δ as a neighbor to Hg may be obtained by interpolating between these cases leading to $V_{zz}^{int}=751$ V/Å^2 and $\eta^{int}=0.17$.

Further calculations were performed with the *overdoped* superlattice with $\delta=0.25$ which is close to the maximum $\delta\sim0.235$ ever found in Hg1201.[11] Due to the much longer computing time needed for this large supercell, full convergence in the self-consistency cycle was not obtained. The extrapolated EFG parameters obtained from the trend in the calculation are shown in Table IV. There are now three different sites for Ba, e.g., Ba*a*, Ba*b*, and a new Ba*c* site that corresponds to Ba atoms which are located *out of* and *farthest away* from O_δ rows. For O(1) there are only two different possibilities e.g., O(1)*b* and O(1)*c* (Fig. 4).

The overall consistency of the EFG calculations has been further cross checked for the *undoped* and *overdoped* superlattices that approximately reproduce the EFG's at the Cu site, as measured by NQR with ^{67}Cu on differently doped Hg1201 materials.[20]

IV. DISCUSSION

By comparing the experimental $|V_{zz}|$ values that were obtained when annealing the samples in Ar (Table II) with the calculated one at the Hg site for the *undoped* cell (Table III), an excellent agreement is found. Therefore, EFG_1 is assigned to Hg atoms at regular Hg1201 lattice sites without O_δ or other defects in the near neighborhood.

The values of $|V_{zz}|$ and η that characterize EFG_2, which

TABLE IV. EFG parameters obtained from FLAPW first-particles calculations on the *saturated* (a) and (b) configurations with $\delta=0.5$ and *overdoped* with $\delta=0.25$ supercells. For the Ba*a* and Ba*c* sites the EFG psa is defined as in Table III when $\eta=0$. For the EFG at the O(1)*a*, O(1)*b*, and O(1)*c* sites the psa is identical to that of O(1) in Table III. For the EFG at the Hg, Ba*b*, Cu, O(2), and O_δ sites, the psa is now defined with the *z* axis parallel to [001], the *x* axis parallel to [110], along the Hg-O_δ direction, and the *y* axis parallel to the [1−10] direction. For the localization of Ba*a*, Ba*b*, Ba*c*, O(1)*a*, O(1)*b*, and O(1)*c* in the unit cell see Fig. 4 and text.

	V_{zz}			V_{yy}			V_{xx}			$\lvert\eta\rvert$		
	Saturated		Overdoped	Saturated		Overdoped	Saturated		Overdoped	Saturated		Overdoped
Element	$Cf(a)$	$Cf(b)$		$Cf(a)$	$Cf(b)$		$Cf(a)$	$Cf(b)$		$Cf(a)$	$Cf(b)$	
Hg	−682.8	−602.8	−760	+457.1	+305.7	+468	+225.7	+297.1	+292	0.339	0.015	0.232
Ba*a*	−110.6	−99.6	−94	+55.3	+50.2	+47	+55.3	+49.4	+47	0	0.008	0.000
Ba*b*	+46.8	+34.0	+46	−23.4	−19.2	−24.5	−23.4	−14.8	−21.5	0	0.129	0.065
Ba*c*			+39			−19.5			−19.5			0.000
Cu	−52.2	−58.0	−13	+26.9	+30.6	+6.5	+25.3	+27.4	+6.5	0.031	0.055	0.000
O(1)*a*		+144.3			−82.1			−62.2			0.138	
O(1)*b*	+154.5	+146.3	+150	−84.0	−84.9	−76.5	−70.5	−61.4	−73.5	0.087	0.161	0.020
O(1)*c*		+144.4	+148		−85.1	−77.7		−59.3	−70.3		0.179	0.050
O(2)	+125.2	+121.5	+131	−67.2	−65.7	−67.5	−58.0	−55.8	−63.5	0.074	0.082	0.030
O_δ	−158.6	−127.2	−86	+79.3	+80.0	+43	+79.3	+47.2	+43	0	0.258	0.000

was found when annealing under oxygen flow, compare well with the EFG parameters calculated for Hg sites with a single near-neighbor O_δ atoms, as calculated with the *overdoped* superlattice and by interpolating between the *undoped* and *saturated* $Cf(a)$EFG estimations. Therefore, EFG_2 is assigned to Hg atoms that have one single oxygen atom in their neighborhood in relative coordinates $(\pm 1/2, \pm 1/2, z_{Hg})$.

At this point it should be stressed that the main contribution for the EFG at the Hg site comes from the tightly bound apical oxygen, O(2), that dominates the influence of the weakly Hg-bound O_δ defect. This is clearly seen in the experimental data, as well in the calculations of the *overdoped* model, where the presence of a single O_δ atom mainly changes the asymmetry parameter ($\eta_2 \neq 0$) of the EFG at the Hg site.

For realistic low O_δ concentrations the PAC fractions should provide information on δ within the implanted region of the sample. The EFG calculations showed that only the *overdoped* configuration explains the fraction f_2 of Hg nuclei interacting with EFG_2. From the atomic point of view f_2 accounts for the Hg atoms that have only one O_δ atom in their neighborhood, which are located at the center of the Hg square. Since four Hg atoms surround each O_δ, the corresponding abundance is given by $\delta_{PAC} = f_2/4 \approx 0.06$.

It should be noted that when annealing under oxygen flow a fraction of ^{199m}Hg atoms interact with an additional and weaker EFG_3. Once f_3 is small, the full characterization and assignment of EFG_3 to a specific Hg-defect configuration cannot be achieved with the present set of data. However, the fact that $|V_{zz_3}| = 413 \pm 49\ V/Å^2$ has a much lower value than expected for configurations of Hg atoms with two O_δ near-neighbors, as predicted by the *saturated* model, hints that EFG_3 cannot be due to simple O_δ defects. Hence, more oxygen-related defects should exist near the Hg planes in unknown configurations and with unknown oxygen content.

Once the PAC experiments were finished, x-ray-diffraction analyses were done on the same samples. These revealed that *a* and *c* have changed as expected, i.e., increasing on the samples which have been annealed under Ar and decreasing on the samples which have been annealed under oxygen flow, relative to the lattice parameters of the *as-prepared* material (Table I).

Looking forward to estimate δ on an independent way from the PAC experiments, Fig. 5 shows the trend of δ as a function of *a*. The continuous line is a parabolic fit to a set of δ values which were experimentally measured by several authors and compiled by Loureiro.[11] Based on this trend and on the x-ray-diffraction data, δ was estimated in the present samples to be $\delta \approx 0.08$ and $\delta \approx 0.11$ after annealing under Ar and O_2, respectively.

It should be noted that from the PAC experiments, which were performed during annealing under Ar flow, no fraction of Hg atoms interacting with O_δ was found ($f_1 = 100\% \Rightarrow \delta_{PAC} = 0$). Only when annealing under oxygen flow was a value for $\delta_{PAC} = 0.06$ found as obtained from the fraction of Hg atoms that interact with single O_δ atoms. In both cases δ_{PAC} is much smaller than δ estimated from the lattice parameters.

Besides the uncertainty that characterizes the systematic trend of Fig. 5, different reasons can explain this difference.

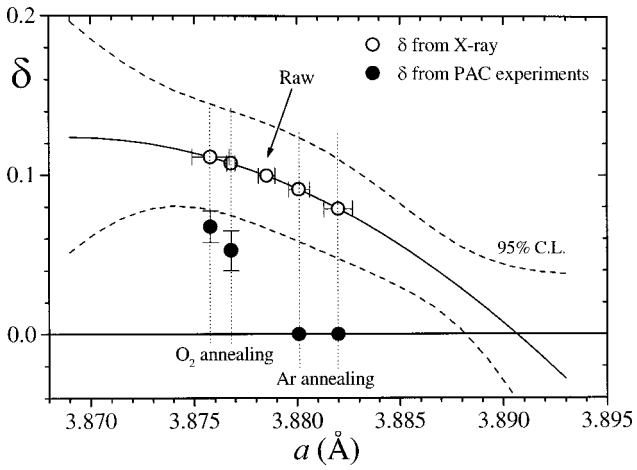

FIG. 5. Trend of δ as a function of the lattice parameter *a*. The continuous line is a parabolic fit to the experimental data collected in Ref. 11. The dotted lines confine the region of the fit within 95% confidence level. For the sake of clearness the experimental points where the fit was done are not included in the figure.

The first one is the fact that the shallow implantation depth of the ^{199m}Hg nuclei is very close to the surface. Consequently, during annealing treatments the ^{199m}Hg probe nuclei are more exposed to oxygen release than the bulk of the samples that is probed by x-ray analysis, resulting in nonhomogeneous O_δ concentration. The second reason has to do with the fact that δ_{PAC} only accounts for those oxygen atoms that exist as single O_δ atoms at the center of the Hg planes without defects nearby. As it was already discussed, the PAC data show that other defect complexes should exist, but, so far, with unknown oxygen content. When using the traditional nonlocal techniques for measuring the oxygen concentration, on which the systematic trend of Fig. 5 is based, single oxygen atoms are not distinguished from other oxygen-related defects. This can lead, in particular, to an overestimation of the concentration of the simple O_δ defect.

V. CONCLUSIONS AND PERSPECTIVES

The EFG's at the Hg site in Hg1201 have been measured with the PAC nuclear technique. Annealing performed under Ar and O_2 flow revealed that the EFG's at the Hg site are quite sensitive to the O_δ doping concentration. After oxygen annealing a value of $\delta_{PAC} = 0.06$ is found, which represents the concentration of O_δ atoms located at the center of the Hg squares. PAC has further revealed that more unidentified oxygen-related defects must be present near the Hg planes. These can lead to a misinterpretation of δ when measured by the more traditional bulk techniques.

EFG first-principles calculations were performed for the undoped and oxygen doped Hg1201 lattice structure. These reproduced well the experimental values obtained for the EFG at the Hg site, as well those which were measured by Machi[20] for the Cu site. The *ab initio* calculations have confirmed that Hg is tightly bound to the apical oxygen, whose contributions dominate the EFG at the Hg site. The calculations have further shown that the EFG at the Ba site is extremely sensitive to the O_δ presence. This fact suggests that an experimental effort should be envisaged to measure the

EFG's at the Ba site, in order to probe the changes of the Ba local charge density and symmetry as a function of doping and temperature.

The reproducibility of the present experiments and the consistency of the theoretical simulations show that PAC experiments on pure and underdoped Hg1201 samples can provide microscopic information about the O_δ doping. Future experiments should provide details on the O_δ diffusion mechanisms as well as on the local behavior of Hg and its electronic environment as a function of temperature.

ACKNOWLEDGMENTS

This work was partially funded by FCT, Portugal, through Project Nos. CERN/S/FIS/1048/98, PBICT/C/CTM/1891/95, and grants under the PRAXIS XXI Program (J.P.A.), and ITN (J.G.C.).

*On leave from Instituto Tecnológico e Nuclear, Estrada Nacional 10, P-2685 Sacavém, Portugal.

[1] S. N. Putilin, E. V. Antipov, O. Chmaissem, and M. Marezio, Nature (London) **362**, 226 (1993); A. Schilling, M. Cantoni, J. D. Guo, and H. R. Ott, *ibid.* **363**, 56 (1993).

[2] L. Gao, Y. Y. Xue, F. Chen, Q. Xiong, R. L. Meng, D. Ramirez, C. W. Chu, J. H. Eggert, and H. K. Mao, Phys. Rev. B **50**, 4260 (1994).

[3] M. H. Julien, P. Carretta, M. Horvatic, C. Berthier, Y. Berthier, P. Ségransan, A. Carrington, and D. Colson, Phys. Rev. Lett. **76**, 4238 (1996); M. H. Julien, M. Horvatic, P. Carretta, C. Berthier, Y. Berthier, P. Ségransan, S. M. Loureiro, and J. J. Capponi, Physica C **268**, 197 (1996); C. H. Booth, F. Bridges, E. D. Bauer, G. G. Li, J. B. Boyce, T. Claeson, C. W. Chu, and Q. Xiong, Phys. Rev. B **52**, R15 745 (1995).

[4] P. Bordet, F. Duc, P. G. Radaelli, A. Lanzara, N. Saini, A. Bianconi, and E. V. Antipov, Physica C **282-287**, 1081 (1997); M. Lagues, C. F. Beuran, C. Hatterer, P. Laffez, V. Mairet, C. Partiot, X. M. Xie, X. Z. Xu, C. Devill Cavellin, B. Eustache, and C. Coussot, in *Coherence in High Temperature Superconductors*, edited by Guy Deutscher and Alex Revcolevschi (World Scientific, Singapore, 1996), pp. 70–98.

[5] A. Lanzara, N. L. Saini, Bianconi, F. Duc, and P. Bordet, Phys. Rev. B **59**, 3851 (1999).

[6] M.-H. Julien, M. Horvatic, P. Carretta, C. Berthier, Y. Berthier, P. Ségransan, S. M. Loureiro, and J. J. Capponi, Physica C **268**, 197 (1996).

[7] H. G. Dehmelt, H. G. Robinson, and W. Gordy, Phys. Rev. **93**, 480 (1954).

[8] Th. Wichert, N. Achziger, H. Metzner, and R. Sielemann, *Perturbed Angular Correlation in Hyperfine Interactions of Defects in Semiconductors* (Elsevier, Amsterdam, 1992), p. 1; T. Butz, Hyperfine Interact. **52**, 189 (1989).

[9] W. Tröger, T. Butz, P. Blaha, and K. Schwarz, Hyperfine Interact. **80**, 1109 (1989).

[10] S. M. Loureiro *et al.*, Physica C **243**, 1 (1995).

[11] (a) S. M. Loureiro, Ph.D. thesis, Université Joseph Fourier, Grenoble, 1997; (b) S. M. Louneiro, J. J. Capponi, E. V. Antipov, and M. Marezio, *On the Synthesis and Structure of* $HgBa_2Ca_{n-1}Cu_nO_{2n+2+\delta}$ *Superconductors*, Studies of High Temperature Superconductors Vol. 25, edited by A. V. Narlikar (Nova Science, New York, 1997), and references therein.

[12] E. Kugler, D. Fiander, B. Jonson, H. Haas, A. Przewloka, H. L. Ravn, D. J. Simon, K. Zimmer, and the ISOLDE Collaboration, Nucl. Instrum. Methods Phys. Res. B **70**, 41 (1992).

[13] J. F. Ziegler, J. P. Biersack, and U. Littmark, *The Stopping and Range of Ions in Solids* (Pergamon, New York, 1985).

[14] W. Tröger and T. Butz, Z. Naturforsch., A: Phys. Sci. **47a**, 12 (1992).

[15] T. Butz, S. Saibene, Th. Fraenzke, and M. Weber, Nucl. Instrum. Methods Phys. Res. A **284**, 417 (1989).

[16] N. P. Barradas, M. Rots, A. A. Melo, and J. C. Soares, Phys. Rev. B **47**, 8763 (1993).

[17] M. Deicher, Hyperfine Interact. **79**, 681 (1993).

[18] P. Blaha, P. Dufek, K. Schwarz, and H. Haas, Hyperfine Interact. **97/98**, 3 (1996); P. Blaha, K. Schwarz, and J. Luitz, WIEN97, Vienna University of Technology 1997 [improved and updated Unix version of the original copyrighted WIEN code, published by P. Blaha. Kschwarz, P. Sonahtin, and S. B. Trickey, Comput. Phys. Commun. **59**, 399 (1990)].

[19] D.-J. Singh, Physica C **212**, 228 (1993).

[20] T. Machi, R. Usami, H. Yamauchi, N. Koshizuka, and H. Yasuoka, Physica C **235-240**, 1675 (1994); W. Hoffmann, H. Breitzke, C. T. Simmons, K. Lüders, G. Buntkowsky, H. H. Limbach, E. V. Antipov, A. A. Gippius, O. Loebich, H. R. Khan, M. Paranthaman, and J. R. Thompson, Appl. Magn. Reson. **8**, 57 (1995); Kunisuke Asayama, Yoshio Kitaoka, Guoqing Zheng, and Kenji Ishida, Prog. Nucl. Magn. Reson. Spectrosc. **28**, 221 (1996); A. A. Gipius, E. V. Antipov, W. Hoffmann, and K. Lüders, Physica C **276**, 57 (1997).